

Published in final edited form as:

*Astron Astrophys.* 2015 May 1; 577: . doi:10.1051/0004-6361/201425338.

## Top-down formation of fullerenes in the interstellar medium

O. Berné<sup>1,2</sup>, J. Montillaud<sup>3,4</sup>, and C. Joblin<sup>1,2</sup>

<sup>1</sup>Université de Toulouse; UPS-OMP; IRAP; Toulouse, France <sup>2</sup>CNRS; IRAP; 9 Av. colonel Roche, BP 44346, F-31028 Toulouse cedex 4, France <sup>3</sup>Department of Physics, PO Box 64, University of Helsinki, 00014, Helsinki, Finland <sup>4</sup>Institut Utinam, CNRS UMR 6213, OSU THETA, Université de Franche-Comté, 41bis avenue de l'Observatoire, 25000 Besançon, France

### Abstract

Fullerenes have been recently detected in various circumstellar and interstellar environments, raising the question of their formation pathway. It has been proposed that they can form at the low densities found in the interstellar medium by the photo-chemical processing of large polycyclic aromatic hydrocarbons (PAHs). Following our previous work on the evolution of PAHs in the NGC 7023 reflection nebula, we evaluate, using photochemical modeling, the possibility that the PAH C<sub>66</sub>H<sub>20</sub> (i.e. circumovalene) can lead to the formation of C<sub>60</sub> upon irradiation by ultraviolet photons. The chemical pathway involves full dehydrogenation of C<sub>66</sub>H<sub>20</sub>, folding into a floppy closed cage and shrinking of the cage by loss of C<sub>2</sub> units until it reaches the symmetric C<sub>60</sub> molecule. At 10'' from the illuminating star and with realistic molecular parameters, the model predicts that 100% of C<sub>66</sub>H<sub>20</sub> is converted into C<sub>60</sub> in ~ 10<sup>5</sup> years, a timescale comparable to the age of the nebula. Shrinking appears to be the kinetically limiting step of the whole process. Hence, PAHs larger than C<sub>66</sub>H<sub>20</sub> are unlikely to contribute significantly to the formation of C<sub>60</sub>, while PAHs containing between 60 and 66 C atoms should contribute to the formation of C<sub>60</sub> with shorter timescales, and PAHs containing less than 60 C atoms will be destroyed. Assuming a classical size distribution for the PAH precursors, our model predicts absolute abundances of C<sub>60</sub> are up to several 10<sup>-4</sup> of the elemental carbon, i.e. less than a percent of the typical interstellar PAH abundance, which is consistent with observational studies. According to our model, once formed, C<sub>60</sub> can survive much longer (> 10<sup>7</sup> years for radiation fields below G<sub>0</sub> = 10<sup>4</sup>) than other fullerenes because of the remarkable stability of the C<sub>60</sub> molecule at high internal energies. Hence, a natural consequence is that C<sub>60</sub> is more abundant than other fullerenes in highly irradiated environments.

### Keywords

astrochemistry; ISM: molecules; molecular processes; Methods: numerical

## 1. Introduction

The mid-infrared (mid-IR) spectrum of galactic and extragalactic objects exhibits emission in bands (strongest at 3.3, 6.2, 7.7, 8.6, and 11.2  $\mu\text{m}$ ) attributed to carbonaceous

macromolecules, more specifically to polycyclic aromatic hydrocarbons (PAHs, Tielens 2008). In addition to PAH bands, IR emission bands at 7.0, 8.5, 17.4, and 19.0  $\mu\text{m}$  have been reported (Cami et al. 2010; Sellgren et al. 2010), and found to match quite closely the IR active bands of neutral buckminsterfullerene ( $\text{C}_{60}$ , Kroto et al. 1985), a cage-like carbon molecule. Additional bands at 6.4, 7.1, 8.2, and 10.5  $\mu\text{m}$  were observed in the NGC 7023 reflection nebula and attributed to the  $\text{C}_{60}^+$  cation (Berné et al. 2013). Carbonaceous macromolecules, especially PAHs, are believed to play a fundamental role in the physics and chemistry of the interstellar medium (ISM), and their infrared signatures are commonly used as a tracer of physical conditions (especially the UV radiation field). PAHs are believed to lock up between 5 and 20% of the elemental carbon (Joblin & Tielens 2011), while  $\text{C}_{60}$  and  $\text{C}_{60}^+$  are found in small abundances in the ISM (at most  $5.6 \times 10^{-4}$  of the elemental carbon for the neutral form according to Castellanos et al. 2014, and at most  $10^{-4}$  of the elemental carbon for the cation according to Berné et al. 2013). Nevertheless,  $\text{C}_{60}$  and  $\text{C}_{60}^+$  are the only species belonging to the family of carbonaceous macromolecules which have been specifically identified in the ISM, and therefore these molecules have attracted considerable interest because they open a new possibility to probe carbon chemistry and physical conditions in the ISM.

One question related to fullerenes, and in particular  $\text{C}_{60}$ , concerns their formation pathway. Recently, “top-down” schemes where larger carbon clusters shrink to reach  $\text{C}_{60}$  have been proposed (Chuvilin et al. 2010; Zhang et al. 2013; Pietrucci & Andreoni 2014), and can be opposed to the traditional “bottom-up” approach where  $\text{C}_{60}$  is built up from small compounds (Kroto & McKay 1988; Heath 1992; Hunter et al. 1994; Dunk et al. 2013). Using infrared observations of the NGC 7023 nebula, Berné & Tielens (2012) found evidence of an increase of the abundance of  $\text{C}_{60}$  with increasing UV field, while the abundance of PAHs decreases. This was interpreted by these authors as evidence for the formation of  $\text{C}_{60}$  from large PAHs ( $N_C > 60$ ) under UV irradiation, a top down mechanism similar to the one observed by Chuvilin et al. (2010). García-Hernández et al. (2010, 2011) and Micelotta et al. (2012) proposed a similar mechanism where the starting materials are more complex, such as hydrogenated amorphous carbon instead of PAHs. Top-down scenarios are particularly appealing, given that the densities prevailing in the ISM are many orders of magnitude too low to allow for a “bottom-up” formation (i.e. starting from small compounds) over reasonable timescales<sup>1</sup>. In this paper, we use a detailed photochemical model coupled to a description of the physical conditions in the NGC 7023 nebula. We demonstrate that the formation of  $\text{C}_{60}$  by UV processing of large PAH molecules is a plausible mechanism to account for astronomical observations.

---

<sup>1</sup>While writing the present paper, it was proposed by Patra et al. (2014) that nucleation of C atoms leading to the formation of cages can operate in the ISM. However, the densities and relative abundances of C and H adopted in this latter work are far from those considered here and actually observed in the interstellar medium.

## 2. Model for the formation of C<sub>60</sub> from PAHs

### 2.1. Description of the proposed scenario

The proposed scenario of formation is inspired by the one described in Berné & Tielens (2012) and is represented schematically in Fig. 1. PAHs are assumed to be formed in the envelopes of evolved stars (Frenklach & Feigelson 1989; Cherchneff et al. 1992; Merino et al. 2014), and then injected in the ISM. Under UV irradiation, large PAHs, ( $N_C > 60$ ) are first fully dehydrogenated into small graphene flakes, dehydrogenation being by far the dominant dissociation channel (see Montillaud et al. 2013, and references therein). Further UV irradiation enables these flakes to fold into closed cages. Once the cages are closed, they can loose C<sub>2</sub> units if they continue absorbing energy (Irlé et al. 2006). Because of the low densities prevailing in the considered regions ( $n_H < 10^4 \text{cm}^{-3}$ ), the reverse reaction, i.e. addition of C<sub>2</sub> is too slow to balance photodissociation. Once a system has reached C<sub>60</sub> it will remain in this form for a very long period of time, because of its remarkable stability.

### 2.2. The specific case of the transformation of C<sub>66</sub>H<sub>20</sub> into C<sub>60</sub>

In this paper we consider the evolution of circumovalene, C<sub>66</sub>H<sub>20</sub> (first molecule in Fig. 1), for the physical conditions of NGC 7023 (see Sect. 3). We restrict ourselves to a single molecule as a starting point, for simplicity, and because modeling a complete population would introduce many free parameters that would be irrelevant in this proof of concept study. C<sub>66</sub>H<sub>20</sub> is selected as a test case because it gathers the typical properties expected for an interstellar PAH ( $N_C \gtrsim 50$ , compactness), it can be considered as a potential precursor of C<sub>60</sub> and its spectroscopic properties are available in the Cagliari Theoretical spectral database of PAHs<sup>2</sup> (Mallocci et al. 2007, hereafter Cagliari database). The photophysical modeling relies on several key processes: 1) UV absorption which brings the molecules to high temperatures, 2) radiative cooling, 3) unimolecular dissociation, 4) isomerization and more specifically folding of the graphene flakes and 5) reactions with electrons, H atoms or C<sup>+</sup>. In the following sections, we present the adopted methods to describe these processes which were then implemented in the photochemical model developed by Montillaud et al. (2013).

**2.2.1. UV absorption**—UV absorption is the first step in the photophysical evolution of the considered species. The efficiency of this process in a given radiation field depends on the UV absorption cross-section. The UV absorption cross-section of C<sub>66</sub>H<sub>20</sub> used here is taken from the Cagliari database. The same value is used for dehydrogenated PAHs C<sub>66</sub>H<sub>*n*</sub> as well as for planar C<sub>66</sub>, considering that the UV absorption cross-section in a PAH is, in first approximation, proportional to the number of carbon atoms. For C<sub>60</sub>, we adopt the UV absorption cross-section from Berkowitz (1999). The same absorption cross-section is used for the other cages, but with a scaling proportional to the number of C atoms (Joblin et al. 1992). The impact of the chosen UV absorption cross-sections on the results is discussed in Sect. 4.3.

<sup>2</sup>[astrochemistry.ca.astro.it/database/](http://astrochemistry.ca.astro.it/database/)

**2.2.2. Ionization**—In the frame of our interstellar model, two ionization processes should be considered: direct photoionization and thermionic emission. Direct ionization occurs after the absorption of a single UV photon with an energy above the ionization threshold. In the case of thermoionic emission, the successive absorption of several UV photons brings the molecule to high temperatures and can lead to delayed electron emission.

For the hydrogenated and dehydrogenated PAHs, the direct photoionization process is included, following Montillaud et al. (2013). For the cages, including  $C_{60}$ , we do not include direct photoionization. This assumption relies on the fact that observations indicate that this species is mostly in the neutral form in NGC 7023,  $C_{60}^+$  being localized only very close to the star (Berné et al. 2013). It cannot be excluded that this is due to an efficient recombination of  $C_{60}$  with electrons from the ambient medium, and hence ionization could still be efficient as a sink of energy for relaxation. Since the ionization potential of  $C_{60}$  is 7.5 eV, only photons with energies  $7.5 < h\nu < 13.6$  eV can contribute to ionization. Given the spectral profile of the radiation field in NGC 7023 (see Montillaud et al. 2013) and the fact that in this range the ionization yield is low compared to the total photo-absorption (Berkowitz 1999), only a small fraction of the energy from absorbed UV photons will be lost in photoelectrons, and most of it will be converted into vibrational energy that can eventually be used for dissociation. The other cages have similar ionization potentials (Seifert et al. 1996) and are therefore assumed to behave like  $C_{60}$ . Hence, we have neglected direct photoionization for the cages in the photo-chemical model.

Thermoionic emission becomes efficient only at internal energies higher than  $\sim 30$  eV (Hansen et al. 2003). It could therefore be an efficient relaxation process, competing with photodissociation (Sect. 2.2.4) and cooling by fluorescence from thermally excited electronic states (Sect. 2.2.3). As can be seen in Fig. 2, the thermoionic emission rate becomes larger than fluorescence from thermally excited electronic states only for internal energies above  $\sim 45$  eV. This is well above the internal energies of dissociation (see Sect. 4.1) and therefore relaxation through thermionic emission can be neglected since it will always be dominated by fluorescence from thermally excited electronic states.

**2.2.3. Radiative cooling**—Radiative cooling can occur through emission of photons in the infrared, but when the molecules reach high enough temperatures, it has been shown that fluorescence from thermally excited electronic states becomes the dominant cooling mechanism (see Léger et al. 1988, who called this mechanism Poincaré fluorescence). This process has been observed for internal energies of  $\sim 7$  eV for the anthracene cation,  $C_{14}H_{10}^+$  (Martin et al. 2013) and internal energies of  $\sim 13$  eV for the  $C_{60}$  anion (Andersen et al. 2001).

The infrared cooling rates are calculated using the microcanonical formalism of Joblin et al. (2002). This requires the full knowledge of the vibrational properties of the considered species. For  $C_{66}H_{20}$ , we use the spectroscopic properties from the Cagliari database as in Montillaud et al. (2013). For  $C_{60}$ , they are taken from Schettino et al. (2001). For dehydrogenated PAHs  $C_{66}H_n$  and cages, we use the DFT vibrational frequencies of  $C_{66}H_{20}$  from the Cagliari database, after removing the C-H vibrational modes and 3 modes per

missing C atom. The cooling rates calculated with this approach for  $C_{60}$  are reported in Fig. 2.

Cooling by fluorescence from thermally excited electronic states is calculated using the formalism described in Chupka & Klots (1997). The cooling rate is given by:

$$k(T) = (2c/a_0) \sum f_i \left( hv_i/mc^2 \right)^2 \exp(-hv_i/k_B T) \quad (1)$$

where  $a_0$  is the Bohr radius,  $f_i$  and  $\nu_i$  are respectively the oscillator strengths and frequencies of the electronic transitions and  $T$  is the temperature of the molecule. For  $C_{66}H_{20}$  and for the dehydrogenated PAHs we use the  $\nu_i$  and  $f_i$  values for  $C_{66}H_{20}$  from the Cagliari database (Table 1). For the cages, we use the energies and oscillator strengths of  $C_{60}$  taken from Chupka & Klots 1997, reproduced in Table 1. Note that these oscillator strengths are a convenient approximation to calculate the radiative cooling but are not true oscillator strengths. Nevertheless, Chupka & Klots (1997) have shown that this approximation is in very good agreement with rate calculations including detailed molecular property information. Using the microcanonical formalism described above for the calculation of the IR cooling rates, we derived the relation between internal energy  $E$  and temperature  $T$  for the different species. Using Eq. 1, this allowed us to derive the radiative cooling rates as a function of  $E$ . For the case of  $C_{60}$  these rates are shown in Fig. 2) and are in good agreement with the earlier work models of Tomita et al. (2003).

#### 2.2.4. Photodissociation: dehydrogenation and shrinking by loss of $C_2$ —

Photodissociation is treated using the statistical approach, and based on the inverse Laplace transform of the Arrhenius equation (see details in Montillaud et al. 2013 and references therein). The parameters involved in this calculation are the activation energy  $E_0$ , the pre-exponential factor  $A$ , and the vibrational densities of states that are computed using the vibrational frequencies. For PAH dehydrogenation (first step in Fig. 1), we use the parameters given in Montillaud et al. (2013). For the shrinking of cages by loss of  $C_2$  molecules (step 3 in Fig. 1), experimental and theoretical results are scarce, except in the case of  $C_{60}$  and  $C_{60}^+$  for which published molecular data have a large scatter, as noticed by Matt et al. (2001). These authors reanalyzed published experiments of  $C_{60}^+$  dissociation and showed that when using similar and consistent sets of molecular data, most experiments lead to similar results, with a pre-exponential factor of  $5 \times 10^{19} s^{-1}$  and a dissociation energy of  $10.0 \pm 0.2$  eV. The activation energy should be equal to the dissociation energy if there is no barrier for the reverse reaction, i.e.  $C_2$  addition. Experimental (Laskin et al. 1997) and theoretical (Yi & Bernholc 1993) studies indeed indicate the absence of such a barrier. More recent studies are generally in line with these results (Diaz-Tendero et al. 2003; Gluch et al. 2004, among others). We consider each shrinking step from  $C_{66}$  to  $C_{58}$  individually (Eqs. 2 to 6 in Table 2). Dissociation energies have been determined theoretically (Zhang et al. 1992) and the values differ significantly from experimental data (Gluch et al. 2004). The theoretical values were computed directly for neutral cages in a consistent manner for all species. In contrast, the experimental values were derived from measurements on fullerene cations. We used the theoretical values in our standard model (Table 2). This choice has the advantage of providing consistent energies for all cages in this study, but with a relatively

high value for  $C_{60}$  (11.1 eV), compared to the results of Matt et al. (2001) (10.0 eV). To reconcile our choice of binding energies with the results of Matt et al. (2001), we adopted a pre-exponential factor of  $2 \times 10^{20} \text{ s}^{-1}$  which leads to a dissociation rate comparable to that of Matt et al. (1999) (their Fig. 8). We used the same factor for the  $C_2$  loss of all cages. The impact of all these assumptions is discussed in Sect. 4.3.

**2.2.5. Folding**—For the folding of the carbon flakes (step 2 in Fig. 1), there are, to our knowledge, no experimental data to constrain the activation energy and pre-exponential factors. Recently, Lebedeva et al. (2012) conducted molecular dynamics simulations of the folding of the  $C_{96}$  and  $C_{384}$  graphene nanoflakes. For these two systems, they ran simulations at several temperatures and found that the rates follow an Arrhenius law from which they were able to derive the effective activation energies and pre-exponential factors. They show that these parameters do not vary significantly with size<sup>3</sup>, hence we adopt their values reported for  $C_{96}$  to describe the folding (see Table 2).

**2.2.6. Reaction with electrons, H atoms or  $C^+$** —The other processes of interest include the recombination with electrons and the reaction with H atoms. During the dehydrogenation step all these processes are included, following Montillaud et al. (2013). We do not include the addition of  $C_2$ , because the abundance of this species is expected to be very low in the cavity of NGC 7023. The  $C^+$  cation is however abundant, and could react efficiently with cages. There are to our knowledge no studies of the kinetics of this reaction. We estimated the maximum contribution of this process in the case of  $C_{60}$  using the Langevin rate. A polarizability of  $\sim 80 \text{ \AA}^3$  for  $C_{60}$  (Zope et al. 2008) leads to  $k_{\text{Langevin}} \sim 6 \times 10^{-9} \text{ cm}^3 \text{ s}^{-1}$ , and assuming a high abundance of  $C^+$  of  $3 \times 10^{-4} n_H$ , one gets an effective  $C^+$  addition rate of  $\sim 2 \times 10^{-12} n_H \text{ s}^{-1}$  (that is  $< 4 \times 10^{-8} \text{ s}^{-1}$  for  $n_H < 2 \times 10^4 \text{ cm}^{-3}$ ). This rate must be compared to the rate of the reverse process, i.e. photodissociation of  $C_{61}^+$ . We modeled this latter process with the same formalism as described in Sect. 3, using a dissociation energy of 4 eV (Slanina & Lee 1994) and a pre-exponential factor of  $1.6 \times 10^{15} \text{ s}^{-1}$  (Klots 1991). We find photodissociation rates from  $\sim 7 \times 10^{-8} \text{ s}^{-1}$  to  $\sim 2 \times 10^{-5} \text{ s}^{-1}$  for the various astrophysical conditions considered in Sect. 4.2. Therefore, the photodissociation of  $C_{61}^+$  is estimated to be generally much faster than  $C^+$  addition in the regions of interest, and we do not include this latter process in our study.

### 3. Astrophysical environment: NGC 7023

Since NGC 7023 is the template interstellar source for the study of fullerene formation (Sellgren et al. 2010; Berné & Tielens 2012; Montillaud et al. 2013), we will model the photochemical evolution of  $C_{66}H_{20}$  for conditions found in this nebula. The formation of  $C_{60}$  is thought to occur inside the cavity between the star HD 200775 and the PDR situated  $40''$  at the North-West of the star. Here, we study five positions at 5, 10, 15, 20 and  $25''$  from the star, situated on a cross-cut (see Fig. 1 in Montillaud et al. 2013) that goes from the star to the PDR. On the same cross-cut, we derive the spectral energy distribution of dust emission using archival data from the *Herschel* space telescope (see Abergel et al. 2010).

<sup>3</sup>It should be noted that this assertion concerns the 100-400 C atoms range and may not extend to lower C numbers, yet as discussed in Sect. 4.3 the activation energy would need to be different from the adopted one by a large factor to alter our results



Using these SEDs, we derive the column density on the line of sight using a value for dust opacity at  $250\ \mu\text{m}$  of  $1.14 \times 10^{-25}\ \text{cm}^2$  per H atom (see details on the method in Planck Collaboration XXV 2011). This yields a column density profile, which we divide by the thickness of the region derived by Pilleri et al. (2012) based on the modeling of the PAH emission profile, i.e. 0.13 pc. The resulting density profile is shown in Fig. 3. To obtain an analytical description of this profile, we fit it with an exponential law (see Fig. 3). The intensities of the radiation field at 5, 10, 15, 20 and 25'' from the star are derived as in Montillaud et al. (2013) and the corresponding profile of  $G_0$  (UV field intensity in terms of the Habing field, which corresponds to  $1.6 \times 10^{-3}\ \text{erg cm}^{-2}\ \text{s}^{-1}$  when integrated between 91.2 and 240 nm, Habing 1968) as a function of distance to the star is presented in Fig. 3. In order to derive the temperature of the gas at these positions PDR modeling is required. For the conditions described above the gas temperature derived by the Meudon PDR model typically ranges between a few 100 and 1000 K. Here we adopt a characteristic temperature of 300 K for the photochemical model but the exact value is not critical (see Sect. 4.3). Finally, a parameter that is key when comparing the results of the model with observations is the age of the nebula, i.e. the time from when the cloud started to receive UV photons. This number cannot be derived directly and hence other indicators have to be used. One is the age of the illuminating star HD 200775. It is difficult to give a precise “age” for such a young and massive star, however, it is most likely ranging between  $10^4$  and  $5 \times 10^5$  years (Alecian et al. 2008, 2013 and Alecian 2014 priv. comm.). Berné & Tielens (2012) adopted a value for the age of the nebula ranging from a few  $10^4$  to  $1 \times 10^5$  years. The analysis of the dynamical properties of the warm neutral gas traced by the  $\text{C}^+$  line with Herschel indicate an age of  $\sim 0.5$  Myrs (Berné et al. 2012). However, more recent calculations focusing on the photo-evaporation flow in the NGC 7023 North PDR indicate ages as low as  $1.6 \times 10^4$  years (Berné et al. in prep). We will use  $10^5$  years as the reference age, but we will consider a range between  $10^4$  and  $5 \times 10^5$  as an age uncertainty range.

## 4. Results

### 4.1. Internal energies

In order to understand the processes at play in the photochemistry, it is useful to evaluate the probability density functions (PDFs) of the internal energies of the species that photodissociate with the model. Fig. 4, shows such a PDF for  $\text{C}_{60}$  at a distance of 5'' from the star. In Table 3, we report the main characteristics of these PDFs for all the cages considered in the model: the peak energy  $E_{peak}$  i.e. the energy of maximum dissociation rate  $D(E)$  expressed in  $\text{s}^{-1}$ , and the lower and upper bounds  $E_{low}$  and  $E_{up}$  defined by  $D(E_{up}) = D(E_{low}) = D(E_{peak})/100$  with  $E_{up} > E_{low}$  (see Fig. 4 for a graphical definition of these parameters). These values are calculated using the activation energies of Zhang et al. (1992), and those of Gluch et al. (2004) (Table 2). The results presented in Table 3 indicate that the internal energies required to dissociate the molecules are high, i.e.  $> 15$  eV. Photons in the NGC 7023 nebula have a maximum energy set by the Lyman limit, i.e. 13.6 eV. Hence, the molecules that dissociate must have absorbed multiple photons, and therefore the photochemistry of these species is completely governed by these multiple-photon absorptions. In the specific case of  $\text{C}_{60}$ , the energy needed is at least 27 eV, i.e. requiring the absorption of at least three photons in order to dissociate.

## 4.2. Abundances

The results of the model are given in Fig. 5 which presents the 20 time-evolution of the

abundance of PAHs ( $\sum_{n=1}^{20} C_{66}H_n$ ), and cages ( $C_{66}^{planar}$ ,  $C_{66}^{cage}$ ,  $C_{64}^{cage}$ ,  $C_{62}^{cage}$ ,  $C_{60}^{cage}$ ,  $C_{58}^{cage}$ ) and  $C_2$ , at distances of 5, 10, 15, 20 and 25'' from the star HD 200775 in NGC 7023. For these five positions, full dehydrogenation occurs very quickly (a few 10s of years at 25'' and a few days at 5'' from the star). This implies that  $C_{66}H_{20}$  is quickly destroyed in NGC 7023, however larger PAHs could survive over longer timescales. Once the planar  $C_{66}$  is formed, it immediately folds and forms a cage. This implies that graphene flakes are only transient species and therefore unlikely to be detected in the ISM. The  $C_{64}$  cage, instead, can survive for a relatively long period of time (few 10s of years at 5'' from the star and up to several  $10^5$  years at 25'' from the star). It is therefore the shrinking step, where cages loose  $C_2$  units, that limits the efficiency of the  $C_{60}$  formation process in this model. Since each of the  $C_2$  loss process is time consuming, it appears unlikely that PAHs with sizes  $N_C \gtrsim 66$  C atoms will contribute significantly to the formation of  $C_{60}$ . At distances shorter than 10'' from the star the cages can shrink to  $C_{60}$  and after  $10^5$  years all the  $C_{66}H_{20}$  has been converted to  $C_{60}$ . Once the molecules have reached  $C_{60}$ , it takes a very long time to destroy them:  $C_{60}$  survives for 10's of Myrs at distance larger than 10'' to the star (radiation fields below  $G_0$  of a few  $10^4$ ). Only at the closest position to the star (5'',  $G_0 \sim 2 \times 10^5$ ) is  $C_{60}$  destroyed efficiently and hence it is predicted that its abundance will decrease after a few  $10^4$  years.

## 4.3. Sensitivity of model results

Is the model very sensitive to the adopted parameters, and if so, which are the critical parameters ?

First, we have checked that the dehydrogenation timescale is always much smaller than the cage formation plus shrinking timescale for the physical conditions of the considered positions. Therefore, it is equivalent to start our calculations with the planar  $C_{66}$  rather than with  $C_{66}H_{20}$ . All the following tests have been conducted with the above assumption, except for the gas temperature test. We first test the choice in the vibrational frequencies for the system. We find the exact values of the frequencies to have a negligible impact on the results, as long as the number of vibrational degrees of freedom and the orders of magnitude of the frequencies are correct. We have varied the gas temperature in the model from 100, to 300 and 1000 K and found that this has a negligible impact on the  $C_{60}$  formation timescale. The UV-visible absorption cross section of the cages, which is not well known, has a somewhat larger impact on the results. For instance, if for the cages we use the cross section per C atom of  $C_{66}H_{20}$  (Mallocci et al. 2007) instead of the one of  $C_{60}$  (Berkowitz 1999), we obtain a variation by a factor of three in the timescale of formation of  $C_{60}$ . Multiplying the pre-exponential factors of  $C_2$  loss by 0.1 or 10 simultaneously for all cages we observe an inversely proportional variation of the  $C_{60}$  formation timescale. This effect in the abundance of  $C_{60}$  is illustrated by the shadowed region in Fig. 5. When varying individually these coefficients, we find that the results are impacted mainly by the value for  $C_{66} \rightarrow C_{64} + C_2$ , and marginally for  $C_{64} \rightarrow C_{62} + C_2$ , while changes for the two other shrinking reactions do not impact the results. We compared our standard results (i.e. using the activation energies



from Zhang et al. 1992) with the results obtained when using the experimental dissociation energies of Gluch et al. (2004). The  $C_{60}$  formation timescales is slightly increased, mainly due to the higher stability of  $C_{66}^{cage}$  in the experimental data set. Overall, the effect does not affect the comparison with observations and discussion which follow. Hence from now on we only consider the results of the model using the activation energies from Zhang et al. 1992. The main source of uncertainty appears to arise from the pre-exponential factors chosen for the shrinking steps. We will therefore consider their effect in the comparison with observations.

## 5. Comparison with observations

In this section we compare the results of our model with the observation of  $C_{60}$  formation in NGC 7023. To be completely accurate, this comparison would require that the model contains a whole size distribution of PAHs in agreement with observations. This requirement is beyond the scope of this paper, but the agreement between the observations and the model can be tested bearing this limitation in mind.

The comparison is primarily based on confronting the maximal abundance of  $C_{60}$  observed in NGC 7023, at a distance of 11'' from the star, with the value obtained in the model for a distance of 10''. Taking into account the uncertainty on the age of NGC 7023 and the uncertainty on the pre-exponential factors, the model-predicted abundances of  $C_{60}$  ranges between a minimum value of  $1.3 \times 10^{-2}$  and 0.98, relative to  $C_{66}H_{20}$  (Fig. 5). To convert this into an absolute abundance of  $C_{60}$  one needs to know the abundance of  $C_{66}H_{20}$  relative to the total PAH population, and to know the total abundance PAHs in NGC 7023. The latter was estimated by Berné & Tielens (2012) to be  $f_C^{PAH} = 7 \times 10^{-2}$  expressed in fraction of carbon locked in PAHs. The maximum abundance of  $C_{66}H_{20}$  relative to the total PAH population,  $\alpha$ , can be estimated following Pilleri et al. (2009), using the PAH size distribution of Desert et al. (1990), which yields a value  $\alpha = 5.3 \times 10^{-3}$ . Thus, the fraction of carbon locked in  $C_{66}H_{20}$  is  $5.3 \times 10^{-3} \times 7 \times 10^{-2} = 3.7 \times 10^{-4}$ . With this value, the fraction of carbon locked in  $C_{60}$  predicted by the model at a distance of 10'' from the star ranges between  $f_C^{C_{60}} = 4.8 \times 10^{-6}$  and  $f_C^{C_{60}} = 3.6 \times 10^{-4}$  (where the lower and upper limit of the range include the uncertainty on the pre-exponential factor and the age of the nebula). This range of values is in agreement with the one derived by Berné & Tielens (2012) of  $f_C^{C_{60}} = 1.7 \times 10^{-4}$ . So far we have considered  $C_{66}H_{20}$  as the only precursor of  $C_{60}$ . As mentioned in Sec. 4.2, it is reasonable to expect that only PAHs bearing between 60 and 66 C-atoms will be able to form  $C_{60}$ , and hence can increase the final abundance of  $C_{60}$ . Hence, it is realistic to calculate  $\alpha$  incorporating all the species bearing between 60 and ~66 C atoms, which yields  $\alpha = 3.8 \times 10^{-2}$ . With this value, the abundance of  $C_{60}$  at 10'' from the star is predicted to range between  $f_C^{C_{60}} = 3.5 \times 10^{-5}$  and  $f_C^{C_{60}} = 2.6 \times 10^{-3}$ , in good agreement with the value derived by Berné & Tielens (2012) of  $f_C^{C_{60}} = 1.7 \times 10^{-4}$ . The comparison can be extended to the other positions (15, 20 and 25'') where the abundance of  $C_{60}$  has been measured. At these three positions, the model derived ranges of abundance are also in good agreement with the observed abundances. However, as the distance grows the range of acceptable values predicted by the model become broader and less constraining.

Overall, the present comparison demonstrates that our scenario is compatible with observations within the uncertainties on the molecular parameters and the age of the nebula.

## 6. Discussion

### 6.1. Comparison to other models

Models of  $C_{60}$  formation in a top-down mechanism were presented in Berné & Tielens (2012) and Micelotta et al. (2012). The scenarios in these papers are quite similar, the main difference being that Berné & Tielens (2012) consider PAHs as the starting ingredient while for Micelotta et al. (2012) it is nanometer-sized “aromatic” clusters. In both of these studies the evolution of the species is described by a “thermal model” (Arrhenius equation), where the driving parameter is the activation energy. For the loss of C atoms at the edge of graphene sheets, Berné & Tielens (2012) used a value tuned to 4.5 eV to obtain reasonable formation efficiencies. Yet, as noted by Micelotta et al. (2012) this value is somewhat arbitrary and the obtained  $C_{60}$  formation efficiencies remain low. To explain the efficient formation of  $C_{60}$  in evolved stars, Micelotta et al. (2012) used the results from the molecular dynamics simulations of Zheng et al. (2007), and extracted a unique activation energy of 0.35 eV for the shrinking reaction by loss of  $C_2$ . However, this value is a factor of  $\sim 20$  smaller than what is generally accepted for this reaction (see Table 1), leading to over-estimations of the rates by many orders of magnitude, casting serious doubts on the conclusions of Micelotta et al. (2012). In summary, since these simple models do not allow the molecules to reach high internal energies through multiple photon absorptions, high formation rates of  $C_{60}$  require activation energies tuned to values that are too low to be physical.

In summary, since these simple models do not consider multiple photon absorptions, the molecules never reach the high internal energies necessary to a high formation rate of  $C_{60}$ . Therefore, they strongly underestimate the  $C_{60}$  formation yields, unless one assumes activation energies that are too low to be physical. Instead, the approach presented here, including a complete description of the photochemical processes, allows, using realistic molecular parameters, to predict formation efficiencies that are in agreement with observations.

### 6.2. Comparison to experimental results of gas-phase cage formation

After we submitted the present paper, Zhen et al. (2014) reported experimental results in which they demonstrate that  $C_{60}$  can be formed in the gas phase through laser irradiation of larger PAH molecules. These results support the idea put forward here that  $C_{60}$  can be formed following a top-down scheme. However, Zhen et al. (2014) suggest that in some cases the conversion of graphene into cages could involve a prior step of  $C_2$  loss. This is in contradiction with our photochemical model in which the dissociation by loss of  $C_2$  is less efficient than the folding by many orders of magnitude, and therefore folding always precedes the loss of  $C_2$ . This is mainly because the activation energy for folding (which relies on molecular parameters derived from molecular dynamics simulations performed by Lebedeva et al. 2012) is a factor of  $\sim 2$  smaller than the activation energy for  $C_2$  loss. Further experimental investigation is necessary, in particular to quantify the activation

energies involved in the folding and C<sub>2</sub> loss by flakes, so that they can be included in our model.

### 6.3. Stability of C<sub>60</sub>

Table 3 demonstrates that C<sub>60</sub> can reach particularly high internal energies. In this state, fluorescence from thermally excited electronic states becomes a very efficient cooling channel, postponing the dissociation and conferring an increased stability to C<sub>60</sub><sup>4</sup>. Hence, in the frame of the top-down mechanism detailed here and because of its remarkable stability, C<sub>60</sub> is expected to be the most abundant of all fullerenes in highly UV irradiated environments in space. It is interesting to note that similar kinetic stability arguments have been put forward (Fedorov et al. 2011) to explain the high abundance of C<sub>60</sub> relative to other fullerenes observed in laboratory experiments (Kroto et al. 1985; Krätschmer et al. 1990). As discussed in Sect. 4.2, C<sub>60</sub> is expected to survive for 10s of Myrs in intense radiation fields. In the diffuse ISM, where the radiation field is several orders of magnitude smaller, C<sub>60</sub> is therefore expected to resist to radiation for even larger timescales. In such conditions, other energetic processes must be invoked to destroy C<sub>60</sub>, such as shocks or cosmic rays.

### 6.4. Isomerization of C<sub>60</sub>

There exists a large number of C<sub>60</sub> isomers, and hence there is *a-priori* no reason for the icosahedral *Ih*-C<sub>60</sub> to be the one present in the ISM. *Ih*-C<sub>60</sub> has the lowest energy amongst all C<sub>60</sub> isomers and the closest isomers lie about 2 eV higher in energy (Raghavachari & Rohlfiing 1992). Upon UV absorption, the isomerization reaction from any C<sub>60</sub> isomer towards *Ih*-C<sub>60</sub> requires only 5.4 eV of activation energy (Yi & Bernholc 1992), and is therefore expected to be fast in the conditions investigated here. Conversely, the isomerization reaction from *Ih*-C<sub>60</sub> to another C<sub>60</sub> isomer requires  $\sim 5.4 + 2 = 7.4$  eV, and will be much slower than the previous reaction. Therefore, relatively quickly, the population of C<sub>60</sub> molecules will be dominated by the icosahedral isomer.

## 7. Conclusions

We have presented the first detailed photochemical modeling of C<sub>60</sub> formation from PAHs in space following a top down scheme. This model is calculated for a single molecule (C<sub>66</sub>H<sub>20</sub>) as a starting point, and the key processes are explicitly described: UV photon absorption (including multiple photon events), radiative cooling and dissociation. Because the involved activation energies in this top-down mechanism are high (especially for the shrinking steps), multiple photon absorptions dominate the photochemistry. Using the physical conditions which prevail in the NGC 7023 reflection nebula, we find that C<sub>60</sub> can be formed from C<sub>66</sub>H<sub>20</sub> over a timescale of about 10<sup>5</sup> years with a high efficiency in highly irradiated regions. Assuming that only PAHs containing between 60 and 66 C atoms are precursors of C<sub>60</sub> and a classical size distribution for PAHs, the comparison between the modeled and observed abundances of C<sub>60</sub> shows a good agreement, within the uncertainties of the model. These uncertainties can be reduced once a better characterization of the

<sup>4</sup>Note that since multiple photon absorptions are rare, most C<sub>60</sub> molecules in the ISM are situated at much lower internal energies and the population-averaged emission at a given time remains dominated by infrared transitions. The visible emission of C<sub>60</sub> in the ISM is therefore probably very weak.

reaction rates of the shrinking of cages is available. While developed for the physical conditions of NGC 7023 as representative of the interstellar medium, the scenario and model described in this paper could also be applied to the irradiated circumstellar gas of planetary nebulae, if the physical conditions in these environments can be characterized in detail.

## Acknowledgements

This work was supported by the CNRS program “Physique et Chimie du Milieu Interstellaire” (PCMI) JM acknowledges the support of the Academy of Finland grant No. 250741, and the support of the University of Franche-Comté through the BQR funding. We also acknowledge support from the European Research Council under the European Union’s Seventh Framework Programme ERC-2013-SyG, Grant Agreement n. 610256 NANOCOSMOS. We acknowledge the referee for constructive comments which improved the quality of this manuscript.

## References

- Abergel A, Arab H, Compiègne M, et al. *A&A*. 2010; 518:L96.
- Alecian E, Catala C, Wade GA, et al. *MNRAS*. 2008; 385:391.
- Alecian E, Wade GA, Catala C, et al. *MNRAS*. 2013; 429:1001.
- Andersen J, Gottrup C, Hansen K, Hvelplund P, Larsson M. *The European Physical Journal D - Atomic, Molecular, Optical and Plasma Physics*. 2001; 17:189.
- Berkowitz J. *The Journal of Chemical Physics*. 1999; 111:1446.
- Berné, O.; Joblin, C.; Deville, Y., et al. SF2A-2012: Proceedings of the Annual meeting of the French Society of Astronomy and Astrophysics. Boissier, S.; de Laverny, P.; Nardetto, N.; Samadi, R.; Valls-Gabaud, D.; Wozniak, H., editors. 2012. p. 507-512.
- Berné O, Mulas G, Joblin C. *A&A*. 2013; 550:L4.
- Berné O, Tielens AGGM. *Proceedings of the National Academy of Science*. 2012; 109:401.
- Cami J, Bernard-Salas J, Peeters E, Malek SE. *Science*. 2010; 329:1180. [PubMed: 20651118]
- Castellanos P, Berné O, Sheffer Y, Wolfire MG, Tielens AGGM. *ApJ*. 2014; 794:83.
- Cherchneff I, Barker JR, Tielens AGGM. *ApJ*. 1992; 401:269.
- Chupka WA, Klots CE. *International Journal of Mass Spectrometry and Ion Processes*. 1997; 167:595.
- Chuvilin A, Kaiser U, Bichoutskaia E, Besley NA, Khlobystov AN. *Nature Chemistry*. 2010; 2:450.
- Desert F-X, Boulanger F, Puget JL. *A&A*. 1990; 237:215.
- Diaz-Tendero S, Alcami M, Martin F. *The Journal of Chemical Physics*. 2003; 119:5545.
- Dunk PW, Adjizian J-J, Kaiser NK, et al. *Proceedings of the National Academy of Sciences*. 2013; 110:18081.
- Fedorov AS, Fedorov DA, Kuzubov AA, et al. *Phys. Rev. Lett*. 2011; 107:175506. [PubMed: 22107538]
- Frenklach M, Feigelson ED. *ApJ*. 1989; 341:372.
- García-Hernández DA, Kameswara Rao N, Lambert DL. *ApJ*. 2011; 729:126.
- García-Hernández DA, Manchado A, García-Lario P, et al. *ApJ*. 2010; 724:L39.
- Gluch K, Matt-Leubner S, Echt O, et al. *The Journal of Chemical Physics*. 2004; 121:2137. [PubMed: 15260767]
- Habing HJ. *Bull. Astron. Inst. Netherlands*. 1968; 19:421.
- Hansen K, Hoffmann K, Campbell EEB. *The Journal of Chemical Physics*. 2003; 119
- Heath, JR. Fullerenes. Hammond, G.; Kuck, V., editors. 1992. p. 1-23.
- Hunter JM, Fye JL, Roskamp EJ, Jarrold MF. *The Journal of Physical Chemistry*. 1994; 98:1810.
- Irle S, Zheng G, Wang Z, Morokuma K. *The Journal of Physical Chemistry B*. 2006; 110:14531. pMID: 16869552. [PubMed: 16869552]
- Joblin C, Leger A, Martin P. *ApJ*. 1992; 393:L79.

- Joblin, C.; Tielens, AGGM., editors. EAS Publications Series; PAHs and the Universe: A Symposium to Celebrate the 25th Anniversary of the PAH Hypothesis; 2011.
- Joblin C, Toubblanc D, Boissel P, Tielens AGGM. *Molecular Physics*. 2002; 100:3595.
- Klots C. *Zeitschrift für Physik D Atoms, Molecules and Clusters*. 1991; 21:335.
- Krätschmer W, Lambl LD, Fostiropoulos K, Huffmanl DR. *Nature*. 1990; 347
- Kroto HW, Heath JR, O'Brien SC, Curl RF, Smalley RE. *Nature*. 1985; 318:162.
- Kroto HW, McKay K. *Nature*. 1988; 331:328.
- Laskin J, Weickhardt C, Lifshitz C. *International Journal of Mass Spectrometry and Ion Processes*. 1997; 161:L7.
- Lebedeva IV, Knizhnik AA, Popov AM, Potapkin BV. *The Journal of Physical Chemistry C*. 2012; 116:6572.
- Léger A, Boissel P, d'Hendecourt L. *Phys. Rev. Lett*. 1988; 60:921. [PubMed: 10037891]
- Mallocci G, Joblin C, Mulas G. *Chemical Physics*. 2007; 332:353.
- Martin S, Bernard J, Brédy R, et al. *Phys. Rev. Lett*. 2013; 110:063003. [PubMed: 23432240]
- Matt S, Echt O, Scheier P, Mrk T. *Chemical Physics Letters*. 2001; 348:194.
- Matt S, Parajuli R, Stamatovic A, et al. *European Journal of Mass Spectrometry*. 1999; 5:477.
- Merino P, Švec M, Martínez JI, et al. *Nature Communications*. 2014; 5
- Micelotta ER, Jones AP, Cami J, et al. *ApJ*. 2012; 761:35.
- Montillaud J, Joblin C, Toubblanc D. *A&A*. 2013; 552:A15.
- Patra N, Král P, Sadeghpour HR. *ApJ*. 2014; 785:6.
- Pietrucci F, Andreoni W. *Journal of Chemical Theory and Computation*. 2014; 10:913. [PubMed: 26580170]
- Pilleri P, Herberth D, Giesen TF, et al. *MNRAS*. 2009; 397:1053.
- Pilleri P, Montillaud J, Berné O, Joblin C. *A&A*. 2012; 542:A69.
- Planck Collaboration XXV. *A&A*. 2011; 536:A25.
- Raghavachari K, Rohlifing CM. *The Journal of Physical Chemistry*. 1992; 96:2463.
- Schettino V, Pagliai M, Ciabini L, Cardini G. *The Journal of Physical Chemistry A*. 2001; 105:11192.
- Seifert G, Vietze K, Schmidt R. *Journal of Physics B: Atomic, Molecular and Optical Physics*. 1996; 29:5183.
- Sellgren K, Werner MW, Ingalls JG, et al. *Astrophys. J*. 2010; 722:L54.
- Slanina Z, Lee S-L. *Journal of Molecular Structure: {THEOCHEM}*. 1994; 304:173.
- Tielens AGGM. *ARA&A*. 2008; 46:289.
- Tomita S, Andersen J, Hansen K, Hvelplund P. *Chemical Physics Letters*. 2003; 382:120.
- Yi J-Y, Bernholc J. *The Journal of Chemical Physics*. 1992; 96
- Yi J-Y, Bernholc J. *Phys. Rev. B*. 1993; 48:5724.
- Zhang BL, Xu CH, Wang CZ, Chan CT, Ho KM. *Phys. Rev. B*. 1992; 46:7333.
- Zhang J, Bowles FL, Bearden DW, et al. *Nature Chemistry*. 2013; 5:880.
- Zhen J, Castellanos P, Paardekooper DM, Linnartz H, Tielens AGGM. *ApJ*. 2014; 797:L30.
- Zheng G, Wang Z, Irle S, Morokuma K. *Journal of Nanoscience and Nanotechnology*. 2007; 7:4.
- Zope RR, Baruah T, Pederson MR, Dunlap BI. *Phys. Rev. B*. 2008; 77:115452.

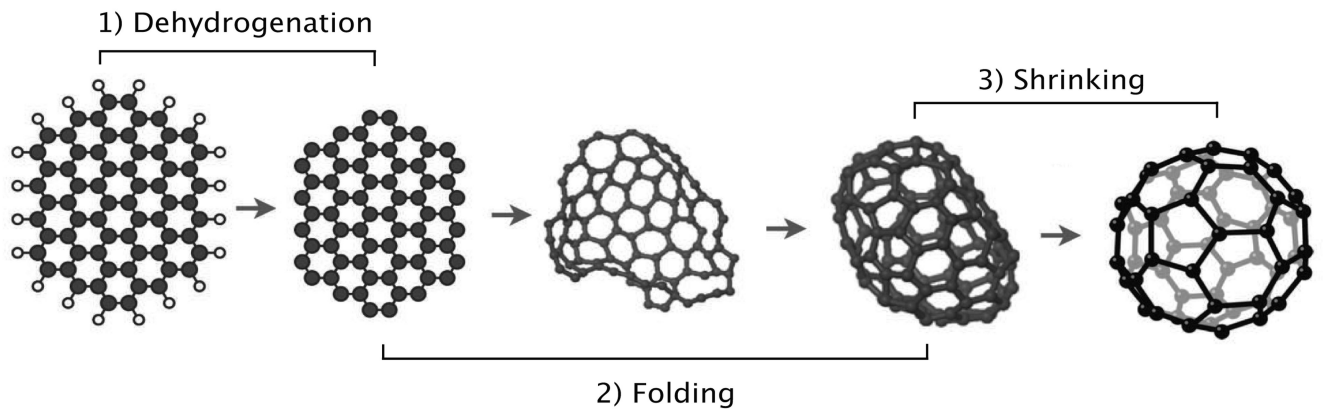


**Fig. 1.** Schematic representation of the evolutionary scenario for the formation of fullerenes from PAHs under UV irradiation.



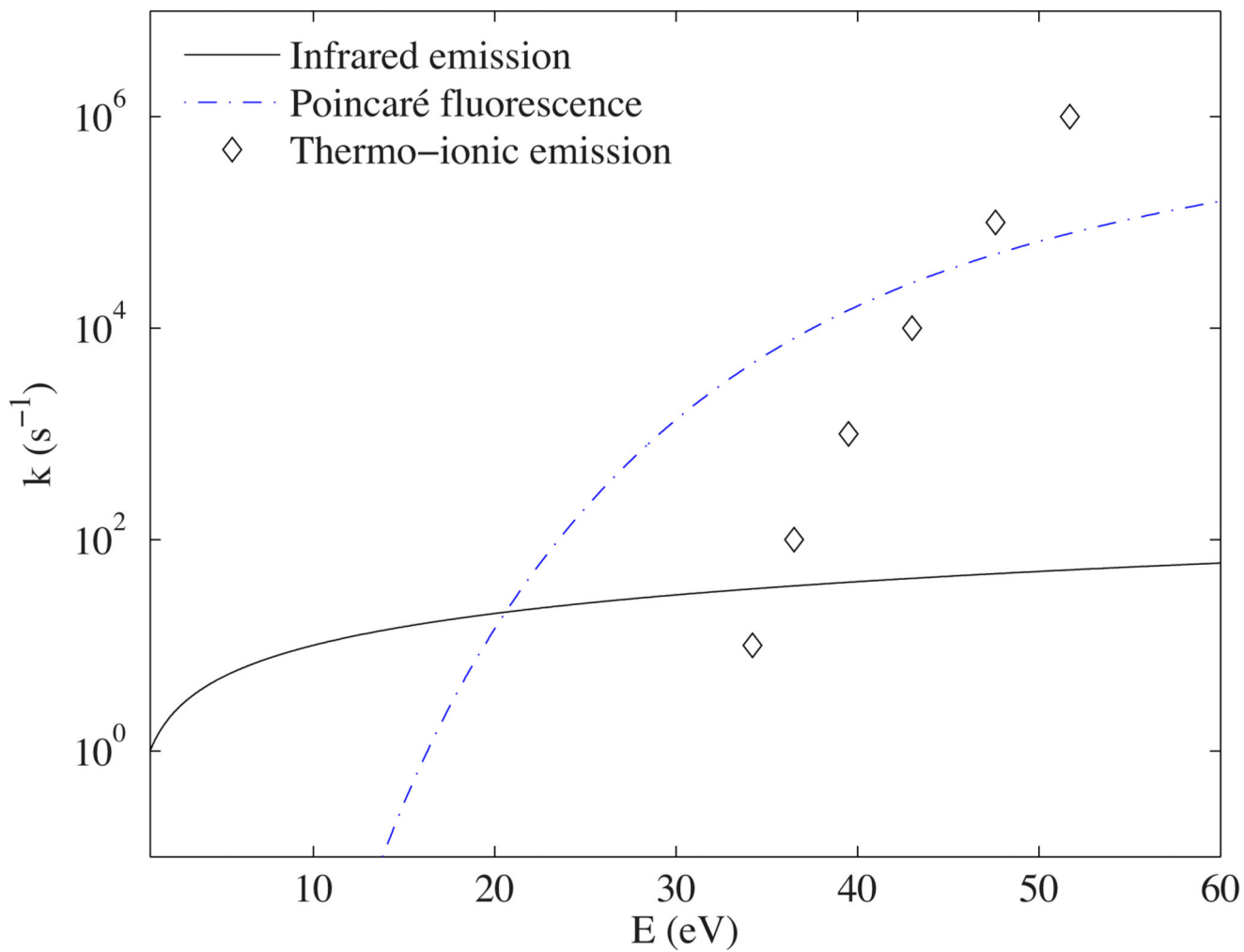


**Fig. 2.** Cooling rates for  $\text{C}_{60}$  as a function of the internal energy of the molecule. The infrared emission and cooling by fluorescence from thermally excited electronic states are calculated (labelled Poincaré in the figure) following the formalism described in this paper. The thermionic emission rates are taken from Hansen et al. (2003).

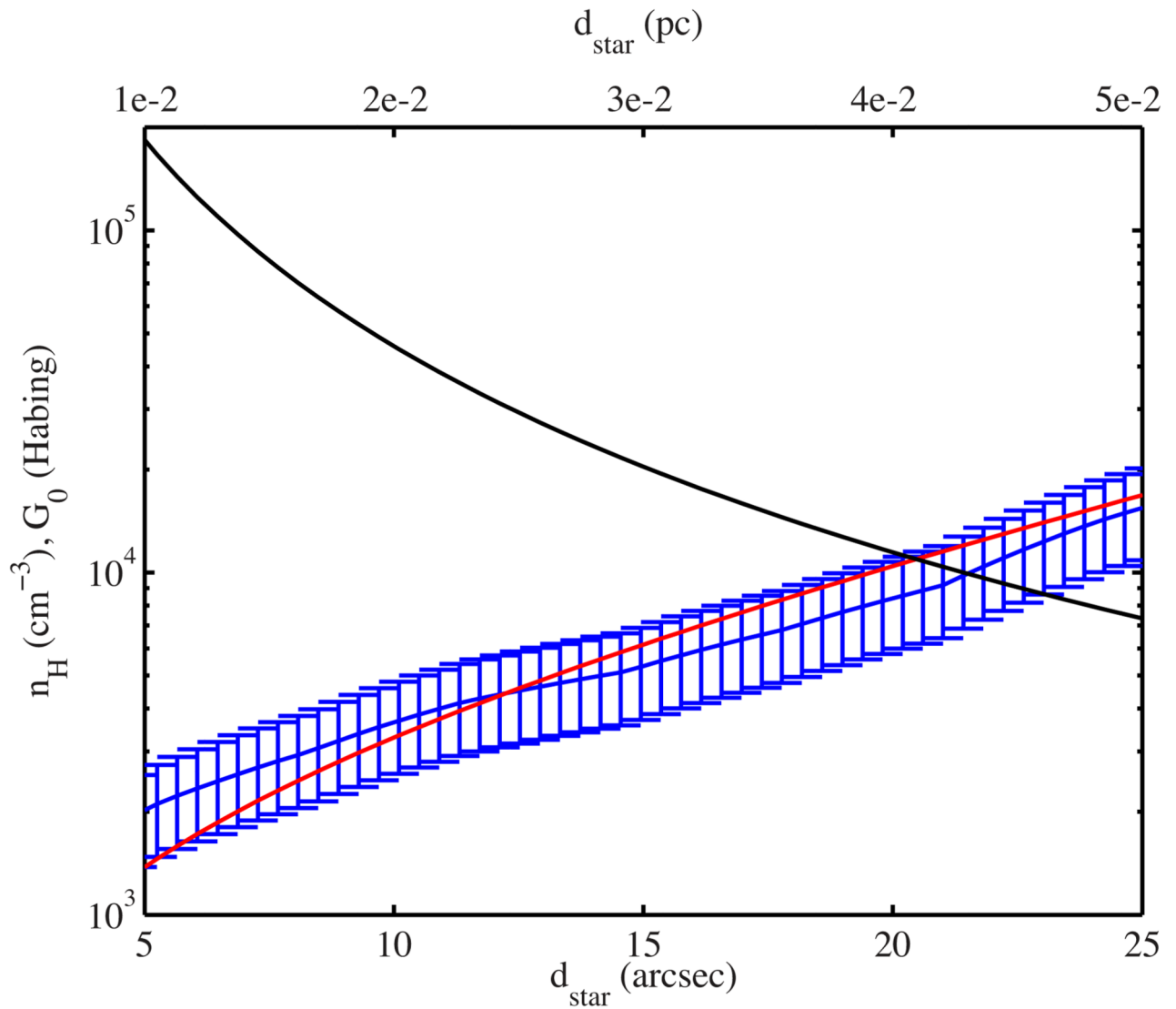


**Fig. 3.** Physical conditions in NGC 7023. Density profile derived from observations of the far-infrared dust emission in the cavity of NGC 7023 (blue with error-bars) and exponential fit to this profile used in the photochemical model (red line). The black line shows the adopted profile for the intensity of the radiation field  $G_0$ .

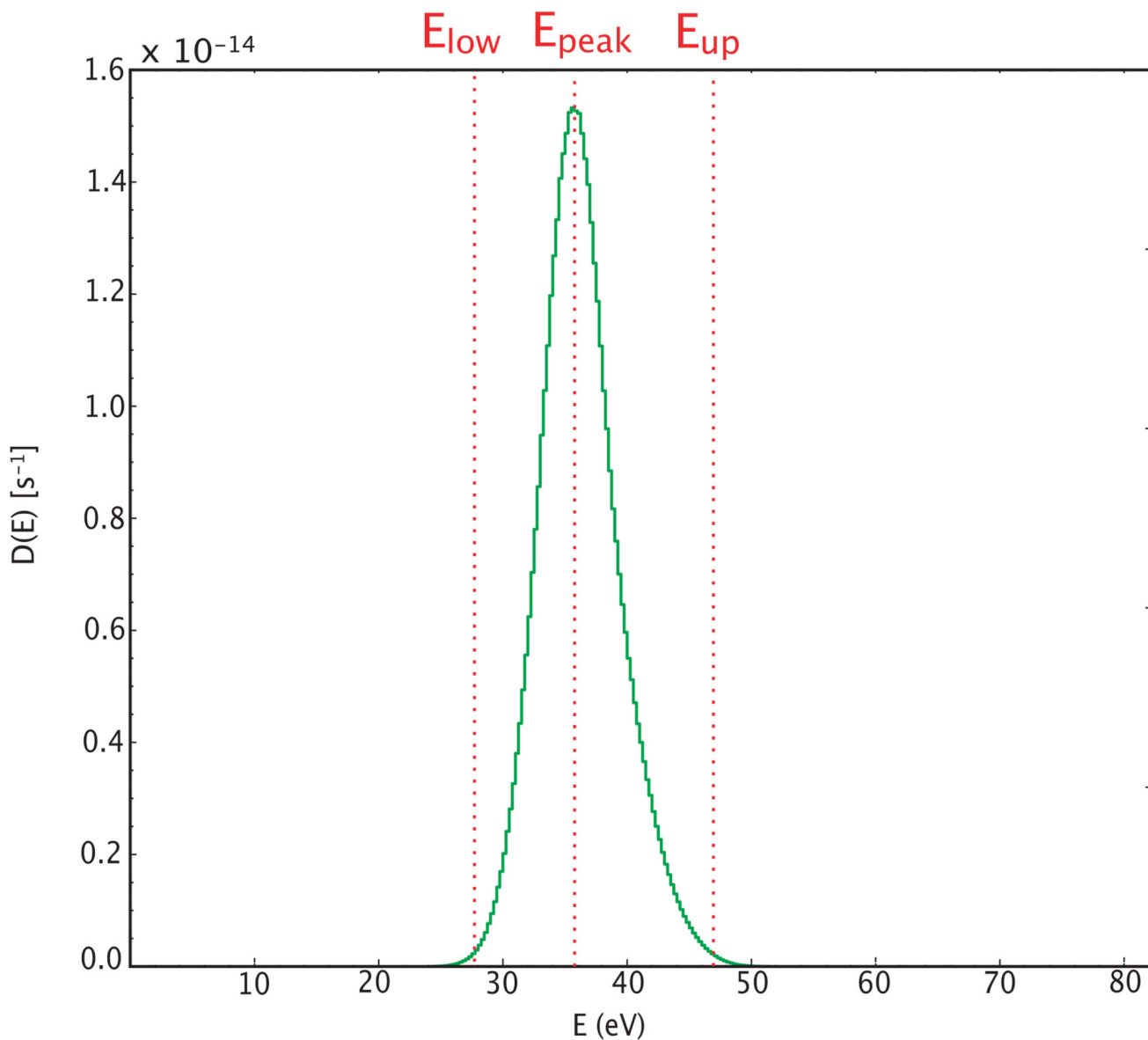


**Fig. 4.** Probability density function of dissociation of the  $\text{C}_{60}$  molecule as a function of internal energy, at a distance of  $5''$  from the star ( $G_0 \sim 2 \times 10^5$ ). Energies  $E_{\text{peak}}$  at maximum dissociation rate ( $D(E) = k_{\text{diss}}(E) \times n(E)$ ),  $E_{\text{low}}$  and  $E_{\text{up}}$  (where  $D(E_{\text{up}}) = D(E_{\text{low}}) = D(E_{\text{peak}})/100$  and  $E_{\text{up}} > E_{\text{low}}$ ) are depicted. The values of  $E_{\text{peak}}$ ,  $E_{\text{low}}$  and  $E_{\text{up}}$  for all cages are given in Table 3.

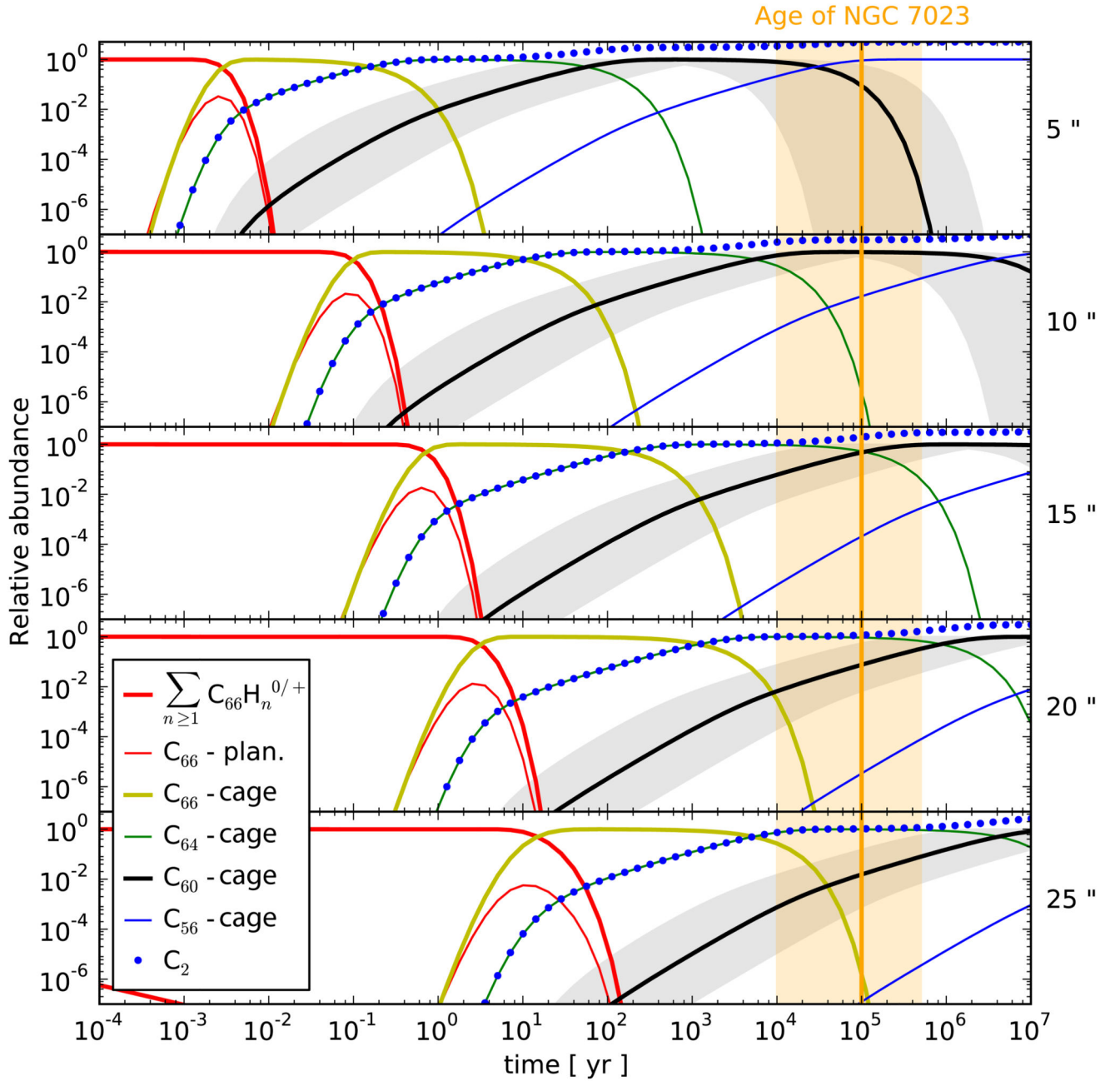


**Fig. 5.**

Model results for the time-evolution of the abundance of PAHs ( $\sum_{n=1}^{20} C_{66}H_n$ ), and cages ( $C_{66}^{planar}, C_{66}^{cage}, C_{64}^{cage}, C_{62}^{cage}, C_{60}^{cage}, C_{58}^{cage}$ ) and  $C_2$ . These are normalized to the abundance of  $C_{66}H_{20}$  at  $t = 0$ . The model calculations are done for distances of 5, 10, 15, 20 and 25" from the star HD 200775 in NGC 7023. Note that the dissociation of  $C_2$  is not treated in our model, hence the  $C_2$  abundances reported are only provided as an indication of how much  $C_2$  is formed from the dissociation of cages. Similarly, the dissociation of the  $C_{56}^{cage}$  is not

included in the model and therefore its abundance is provided as an indication of how much  $C_{60}$  is being destroyed. The gray shadowed regions indicate the uncertainty range implied by uncertainties of a factor of 10 on the rates of  $C_2$  loss (see Sect. 4.3 for details). The approximate age of NGC 7023 is given, with orange shadowed regions representing the uncertainty on this value (see Sect. 3 for details).

**Table 1**

Frequencies and oscillator strengths adopted in the approximation to calculate the cooling by fluorescence from thermally excited electronic states (see text for details).

$\lambda(\text{\AA})$	$\nu_i$ (Hz)	$f_i$
<b>C<sub>66</sub>H<sub>20</sub></b>		
5470	$5.48 \times 10^{14}$	0.72
4980	$6.02 \times 10^{14}$	0.24
<b>C<sub>60</sub></b>		
4540	$6.60 \times 10^{14}$	0.214
3485	$8.60 \times 10^{14}$	1.17
2725	$1.10 \times 10^{15}$	2.02
2240	$1.34 \times 10^{15}$	1.30



**Table 2**

Activation energy and pre-exponential factors for the key reactions considered in the model

		Act. energy $E_a$ (eV)	Pre-exp. factor $A$ ( $s^{-1}$ )
(1)	$C_{66}^{planar} \rightarrow C_{66}^{cage}$	4.0	$1 \times 10^{15}$
(2)	$C_{66}^{cage} \rightarrow C_{64}^{cage} + C_2$	$8.1^a / 9.4^b$	$2 \times 10^{20}$
(3)	$C_{64}^{cage} \rightarrow C_{62}^{cage} + C_2$	$9.4^a / 9.0^b$	$2 \times 10^{20}$
(4)	$C_{62}^{cage} \rightarrow C_{60}^{cage} + C_2$	$6.0^a / 8.1^b$	$2 \times 10^{20}$
(5)	$C_{60}^{cage} \rightarrow C_{58}^{cage} + C_2$	$11.1^a / 11.2^b$	$2 \times 10^{20}$
(6)	$C_{58}^{cage} \rightarrow C_{56}^{cage} + C_2$	$8.7^a / 9.7^b$	$2 \times 10^{20}$

<sup>a</sup>Notes. Using activation energies of Zhang et al. (1992);

<sup>b</sup>Using activation energies of Gluch et al. (2004).

**Table 3**

Properties of the probability density functions of dissociation of cages (see example of such a function in Fig. 4) :  $E_{peak}$ ,  $E_{low}$  and  $E_{up}$ . All values in eV and derived for a distance of 5'' from the star ( $G_0 \sim 2 \times 10^5$ ).

Species*	$a.$			$b.$		
	$E_{low}$	$E_{peak}$	$E_{up}$	$E_{low}$	$E_{peak}$	$E_{up}$
C <sub>66</sub>	22	32	39	26	35	43
C <sub>64</sub>	24	35	43	24	34	41
C <sub>62</sub>	15	20	28	22	30	36
C <sub>60</sub>	27	36	47	27	36	47
C <sub>58</sub>	22	30	37	24	33	41

\* **Notes.** Cages only are presented in this table.

<sup>a</sup> Using activation energies of Zhang et al. (1992);

<sup>b</sup> Using activation energies of Gluch et al. (2004).